REPORT DOCUMENTATION PAGE

Form Approved OMB No. 0704-0188

1. AGENCY USE ONLY (Leave blank)	2. REPORT DATE	3. REPORT TYPE AND DATES COVERED
	12 Mar 85	Conference Presentation

4. TITLE AND SUBTITLE

Unsteady Surface Pressure Measurements on a Pitching Airfoil

5. FUNDING NUMBERS

TA 2307-F1-38

6. AUTHOR(S)

J. Walker, H. Helin, and D. Chou

7. PERFORMING ORGANIZATION NAME(S) AND ADDRESS(ES)

F.J. Seiler Research Laboratory
USAF Academy CO 80840-6528

8. PERFORMING ORGANIZATION REPORT NUMBER

FJSRL-PR-90-0003

AD-A227 905

9. SPONSORING/MONITORING AGENCY NAME(S) AND ADDRESS(ES)

10. SPONSORING/MONITORING AGENCY REPORT NUMBER

11. SUPPLEMENTARY NOTES

12a. DISTRIBUTION/AVAILABILITY STATEMENT

Distribution Unlimited

12b. DISTRIBUTION CODE

13. ABSTRACT (Maximum 200 words)

Surface pressure measurements were taken in an experimental investigation of energetic dynamic stall vortices. The associated unsteady flowfield was generated by a 6-in. NACA 0015 airfoil pitching at high rates to large angles of attack. The airfoil pitch rates varied from 230 deg/sec to 1380 deg/sec and angles of attack varied from zero degrees to 60 degrees. Pitching occurred about its quarter-chord axis. Pitch rate, Reynolds number, and the non-dimensional pitch rate, alpha plus, were varied to determine the effects on pressure and lift coefficients. It was found that increases in pitch rate and Reynolds number had inverse effects on the flowfield in the immediate vicinity of the airfoil. Maintenance of a constant non-dimensional pitch rate produced very similar flowfields and pressure coefficients.

14. SUBJECT TERMS	15. NUMBER OF PAGES
dynamic loads/ aerodynamics vortices. (J/HD)	13
	16. PRICE CODE

17. SECURITY CLASSIFICATION OF REPORT	18. SECURITY CLASSIFICATION OF THIS PAGE	19 SECURITY CLASSIFICATION OF ABSTRACT	20. LIMITATION OF ABSTRACT
UNCLASSIFIED	UNCLASSIFIED	UNCLASSIFIED	NONE

GENERAL INSTRUCTIONS FOR COMPLETING SF 298

The Report Documentation Page (RDP) is used in announcing and cataloging reports. It is important that this information be consistent with the rest of the report, particularly the cover and title page. Instructions for filling in each block of the form follow. It is important to ***stay within the lines*** to meet ***optical scanning requirements***.

Block 1. Agency Use Only *(Leave blank)*.

Block 2. Report Date. Full publication date including day, month, and year, if available (e.g. 1 Jan 88). Must cite at least the year.

Block 3. Type of Report and Dates Covered. State whether report is interim, final, etc. If applicable, enter inclusive report dates (e.g. 10 Jun 87 - 30 Jun 88).

Block 4. Title and Subtitle. A title is taken from the part of the report that provides the most meaningful and complete information. When a report is prepared in more than one volume, repeat the primary title, add volume number, and include subtitle for the specific volume. On classified documents enter the title classification in parentheses.

Block 5. Funding Numbers. To include contract and grant numbers; may include program element number(s), project number(s), task number(s), and work unit number(s). Use the following labels:

C	- Contract	PR	- Project
G	- Grant	TA	- Task
PE	- Program Element	WU	- Work Unit Accession No.

Block 6. Author(s). Name(s) of person(s) responsible for writing the report, performing the research, or credited with the content of the report. If editor or compiler, this should follow the name(s).

Block 7. Performing Organization Name(s) and Address(es). Self-explanatory.

Block 8. Performing Organization Report Number. Enter the unique alphanumeric report number(s) assigned by the organization performing the report.

Block 9. Sponsoring/Monitoring Agency Name(s) and Address(es). Self-explanatory.

Block 10. Sponsoring/Monitoring Agency Report Number. *(If known)*

Block 11. Supplementary Notes Enter information not included elsewhere such as: Prepared in cooperation with...; Trans. of.. ; To be published in.... When a report is revised, include a statement whether the new report supersedes or supplements the older report.

Block 12a. Distribution/Availability Statement. Denotes public availability or limitations. Cite any availability to the public. Enter additional limitations or special markings in all capitals (e.g. NOFORN, REL, ITAR).

- **DOD** - See DoDD 5230.24, "Distribution Statements on Technical Documents."
- **DOE** - See authorities.
- **NASA** - See Handbook NHB 2200.2.
- **NTIS** - Leave blank.

Block 12b. Distribution Code.

- **DOD** - Leave blank.
- **DOE** - Enter DOE distribution categories from the Standard Distribution for Unclassified Scientific and Technical Reports.
- **NASA** - Leave blank
- **NTIS** - Leave blank.

Block 13. Abstract. Include a brief *(Maximum 200 words)* factual summary of the most significant information contained in the report.

Block 14. Subject Terms. Keywords or phrases identifying major subjects in the report.

Block 15. Number of Pages. Enter the total number of pages.

Block 16. Price Code. Enter appropriate price code *(NTIS only)*.

Blocks 17. - 19. Security Classifications. Self-explanatory. Enter U.S. Security Classification in accordance with U.S. Security Regulations (i.e. UNCLASSIFIED). If form contains classified information, stamp classification on the top and bottom of the page.

Block 20. Limitation of Abstract. This block must be completed to assign a limitation to the abstract. Enter either UL (unlimited) or SAR (same as report). An entry in this block is necessary if the abstract is to be limited. If blank, the abstract is assumed to be unlimited.

AIAA'85

AIAA-85-0532
Unsteady Surface Pressure Measurements on a Pitching Airfoil

J. Walker, Frank J. Seiler Research Laboratory USAF Academy, CO, H. Helin, USAF Academy, and D. Chou, Univ. of New Mexico, Albuquerque, NM

AIAA Shear Flow Control Conference

March 12-14, 1985/Boulder, Colorado

UNSTEADY SURFACE PRESSURE MEASUREMENTS ON A PITCHING AIRFOIL

John M. Walker*
Henry E. Helin**
David C. Chou***
Frank J. Seiler Research Laboratory
USAF Academy
Colorado Springs, Colorado 80840-6528

Abstract

Surface pressure measurements were taken in an experimental investigation of energetic dynamic stall vortices. The associated unsteady flowfield was generated by a 6-in. NACA 0015 airfoil pitching at high rates to large angles of attack. The airfoil pitch rates varied from 230 °/sec to 1380°/sec and angles of attack varied from 0° to 60°. Pitching occurred about its quarter-chord axis. Pitch rate, Reynolds number, and the non-dimensional pitch rate, α^+ , were varied to determine the effects on pressure and lift coefficients. It was found that increases in pitch rate and Reynolds number had inverse effects on the flowfield in the immediate vicinity of the airfoil. Maintenance of a constant non-dimensional pitch rate produced very similar flowfields and pressure coefficients.

Introduction

As pointed out by McCroskey,[1] the energetic nature of the unsteady flowfields has been a topic of study for most of the twentieth century. Because of their complicated, rapidly changing time dependent nature, only recently has significant progress been made in theoretical and experimental efforts to understand the fluid mechanics of these flowfields. To continue this progress it is increasingly important not only to be able to predict the onset of dynamic stall but to understand its dynamic nature. Exploitation of dynamic stall increases in aerodynamic coefficients awaits such understanding. The importance of dynamic stall has been well known for years with regard to predicting onset for helicopter rotors, turbo-machinery, and vertical axis wind turbines. A large part of the exploitation emphasis has received impetus from the studies of Herbst[2] into the "supermaneuverability" of fighter aircraft. Understanding of highly unsteady flowfields has been hampered by two things: absence of accurate analytical methods - short of full Navier-Stokes solutions which are only now becoming viable - to predict these flowfields and lack of experimental data needed to set modeling parameters and to verify theoretical calculations.

Most of the experimental data on unsteady flows about pitching airfoils to date have been restricted to sinusoidally oscillating models undergoing relatively small amplitude motions (up to ± 10°) about relatively low mean angles of attack (0° - 15°). These are typified by the experiments of McCroskey and Philippe[3], McAlister and Carr[4], Martin, et. al.[5], and Robinson and Luttges[6]. These data include flow visualization, hot-wire, and pressure measurements and are applicable to many fluid devices of importance. With the exception of Robinson and Luttges[7], however, these studies have not been directed toward the idea that the extremely energetic nature of the unsteady flowfields could be used to enhance performance. Carr, et. al.[8] have shown that lift, drag, and moment coefficients associated with unsteady flowfields greatly exceed their static counterparts. There has, however, been a limited amount of experimental data obtained from tests of very large amplitude motions that will be required if the maneuvers proposed by Herbst[2] (using angles of attack in excess of 45°) are to be implemented.

Studies of moderate to large amplitude constant rate motions have been performed by Harper and Flanigan[9] who obtained force balance data on a small model pitching up to 30°, Francis, et. al,[11] who obtained surface pressure measurements on airfoils pitching up to 60°, Deekins and Kuebler[12], who obtained flow visualization of dynamic leading edge separation at low Reynolds numbers in a smoke tunnel, Daley[13], who obtained leading edge dynamic stall data at low Reynolds numbers, and Walker, et. al.[14] and Helin and Walker[15], who obtained flow visualization using a smoke-wire and near surface hot-wire velocity magnitude data on an airfoil pitching up to 60°. It is clear that

* Major, USAF, Chief, Aeromechanics Division, Member AIAA
** 1Lt, USAF, Instructor, USAF Academy, Member AIAA
*** Professor of Mechanical Engineering University of New Mexico, Albuquere, NM Member AIAA

there is an extensive amount of experimental effort yet to be performed to obtain a clear understanding of the fluid dynamic mechanisms precipitating the occurrence of the dynamic vortices associated with the unsteady flowfields surrounding airfoils pitching at high rates to large angles of attack. It is the intent of this experimental effort to produce definitive lift data for a well defined but limited parameter range of pitch rates and Reynolds numbers. Such definitive results are crucial modeling tools and important assets to a full understanding of the potential of dynamic stall vortices.

Experimental Arrangement

All data were obtained in the USAF Academy Aeronautics Laboratory low-speed, 2 ft x 3 ft subsonic wind tunnel. The model used was a full span, 6 inch chord, NACA 0015 airfoil. The airfoil was instrumented with eighteen Endevco 8507-2 miniature pressure transducers close-coupled to the surface ports, as shown in Figure 1. The signals from each transducer were amplified through Dynamics 7512B amplifiers. The pitching motions of the airfoil were generated by a PDP 11/03 computer controlling a Control Systems Research Index-Syn stepper motor/driver system. This is a modified version of the two-degree-of-freedom oscillator developed by Francis, et. al.[16]. The PDP 11/03 was slaved to a PDP 11/45 which performed the supervisory control and data acquisition. Since the airfoil motions were very repeatable, all eighteen pressure ports were located on one side of the airfoil for better data resolution. This resulted in some minor errors in the data between the upper and lower surfaces due to difficulties in returning the tunnel to the precise flow speed for the opposite surface after turning the airfoil over. The reversal of the airfoil was necessitated by the fact that the stepping motor would turn in only one direction.

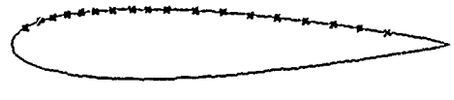

Figure 1. Pressure Port Locations

Experiments were conducted employing a variety of constant rate pitching motions and flow speeds. Table 1 shows the experimental matrix with given in deg/sec and U_∞ in ft/sec, and with the interior values given by the non-dimensional pitch rate parameter $\alpha^+ = \dot{\alpha}\, c/U_\infty$. All of the motions were performed by pitching the airfoil from angles of attack of zero degrees to sixty degrees and stopping. See Figure 2.

Table 1.

$\dot{\alpha}$ (°/s)	230	460	920	1380
U_∞(f/s)				
20	0.1	0.2	0.4	0.6
40		0.1	0.2	
60				0.2
80		0.05	0.1	

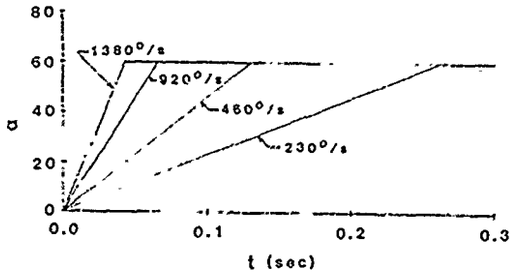

Figure 2. Angle of attack versus time

The Reynolds number based on chord varied from 47500 to 190000. The major objectives of these experiments were to examine the effects of varying pitch rate at constant Reynolds number, varying Reynolds number at constant pitch rate, and holding α^+ constant while varying both pitch rate and Reynolds number. For the nine cases shown in Table 1, data were taken for both surfaces of the airfoil by performing twenty-five repetitions of the pitching motions, taking 200 data points per sensor, and taking the ensemble average.

Experimental Results

The objectives of these experiments were to examine the unsteady aerodynamics surrounding a pitching airfoil and the time dependent fluid mechanics associated with varying pitch rate, Reynolds number, and the non-dimensional pitch rate parameter, α^+. The matrix shown in Table 1, above, was designed to accomplish this task within the experimental constraints of the control, instrumentation, and data acquisition system. The pressure data were used to calculate pressure

coefficients which were in turn integrated to compute lift coefficients. Both types of curves were plotted in the usual way: C_p vs x/c and C_l vs α. In all cases, since these experiments were limited to a single airfoil, varying the Reynolds number is synonymous with varying the flow velocity in the tunnel.

Section Lift Coefficient versus Alpha: The effect of varying the pitch rate while holding Reynolds number constant is dramatic, particularly at the lower flow velocities. At Re = 47500, $C_{l_{max}}$ is a strong function of pitch rate, varying from 2 to 4.3 as pitch rate is increased from 230°/s to 1380°/s. At this Reynolds number, $dC_l/d\alpha$ is also a strong function of pitch rate, varying from 4.3/rad to 8/rad. As Reynolds number increases to 95000 and 190000, however, their dependence is less pronounced. Figure 3 shows C_l vs α for various pitch rates at three different Reynolds numbers, and Figure 4 shows the effect on $C_{l_{max}}$ of increasing pitch rate at constant Re.

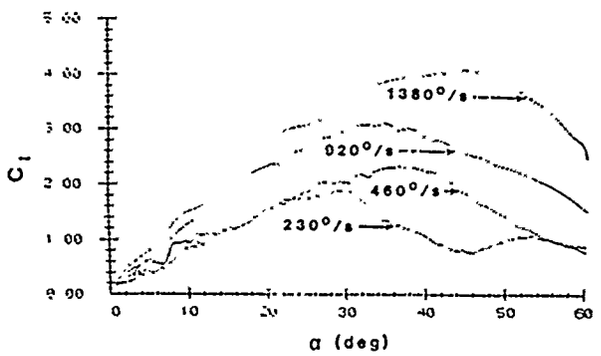

(a) U_∞ = 20 ft/sec,
$\dot{\alpha}$ = 230, 460, 1380 deg/sec

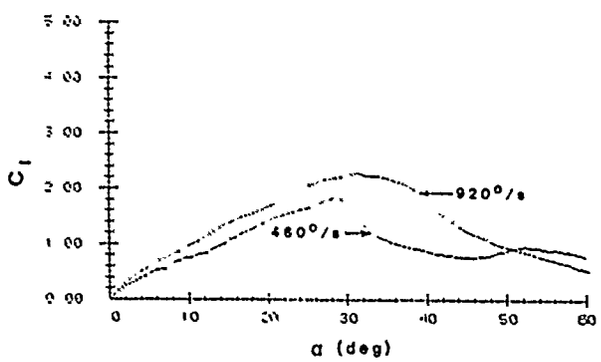

(b) U_∞ = 40 ft/sec
$\dot{\alpha}$ = 460, 920 deg/sec

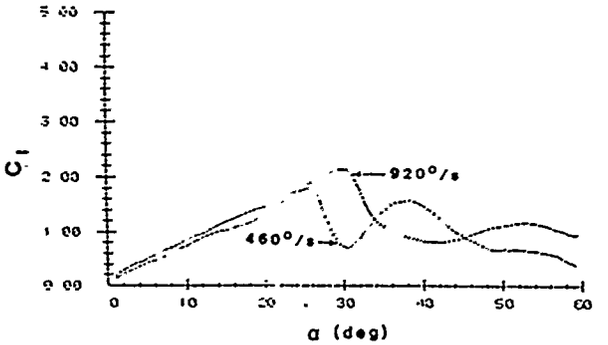

(c) U_∞ = 80 ft/sec
$\dot{\alpha}$ = 460, 920 deg/sec

Figure 3. C_l vs α for constant U_∞ at various pitch rates

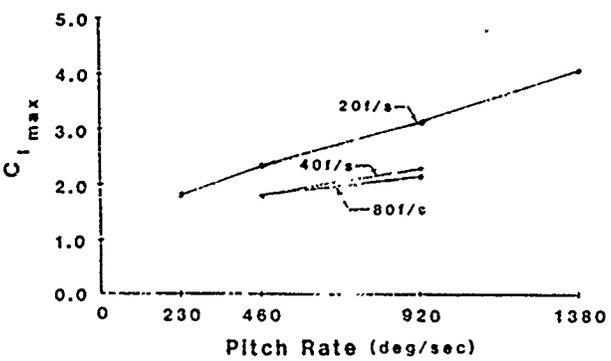

Figure 4. $C_{l_{max}}$ vs $\dot{\alpha}$ at various Reynolds numbers

Figure 4 shows (from Figure 3(a) only) a near linear increase in $C_{l_{max}}$ with respect to pitch rate. Gormont[17] and Strickland and Graham[18] have shown a square root dependency on non-dimensional pitch rate for inception of dynamic stall. Gormont also shows a similar correlation for lift stall. In addition, Walker, et. al.[14] and Helin and Walker[15] presented near-surface hot-wire data that, though being impossible to calculate lift coefficients from, indicate support for this conclusion. While, for steady flows, there is a direct correlation between $C_{l_{max}}$ and stall, it is interesting to note that for these types of unsteady flows, it is not straightforward. In addition to the effect of pitch rate on $C_{l_{max}}$, there is a general dependence of the slope of the lift curve and of the angle of attack at which $C_{l_{max}}$ occurs; and again, this dependence is less pronounced as Reynolds number increases.

The effect of varying Reynolds number while holding pitch rate constant is rather the opposite. $C_{l_{max}}$ is reduced

significantly when increasing Reynolds number from 47500 to 95000 or 142500, but is only slightly affected by increasing Re from 95000 to 190000. Figure 5 shows C_l vs α for various Reynolds numbers at three different pitch rates, and Figure 6 shows the effects on $C_{l_{max}}$ of increasing Re at constant pitch rate. The angle of attack at which $C_{l_{max}}$ occurs is also inversely dependent on Reynolds number, and so, as one would by now expect, is $dC_l/d\alpha$ for rotation rates of 920 and 1380°/s. Oddly enough, however, the lift curve slopes at the pitch rate of 460°/s are all much the same.

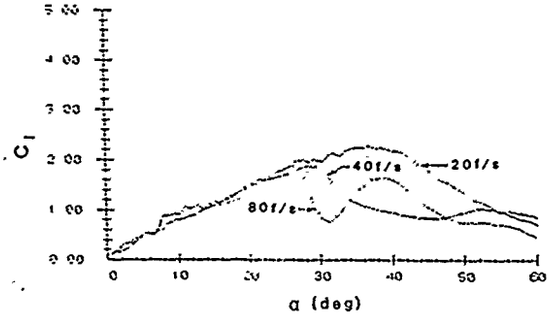

(a) $\dot{\alpha}$ = 460 deg/sec,
U_∞ = 20, 40, 80 ft/sec

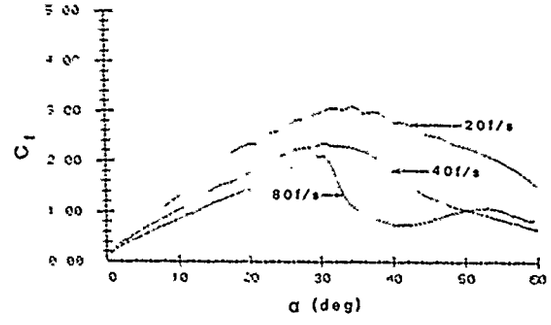

(b) $\dot{\alpha}$ = 920 deg/sec,
U_∞ = 20, 40, 80 ft/sec

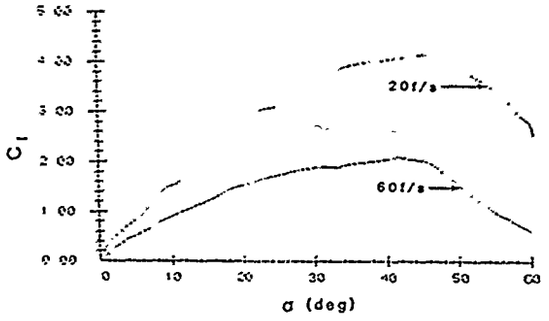

(c) $\dot{\alpha}$ = 1380 deg/sec,
U_∞ = 20, 60 ft/sec

Figure 5. C_l vs α at constant pitch rate for various U_∞

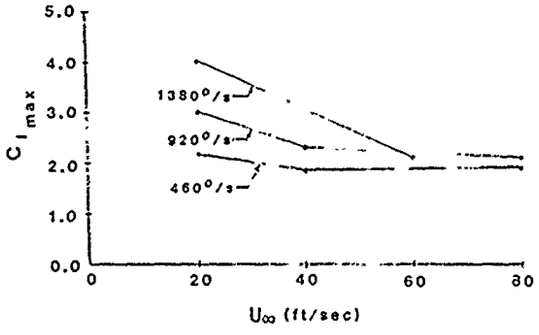

Figure 6. $C_{l_{max}}$ vs U_∞ at various pitch rates

The effect of maintaining the non-dimensional pitch rate parameter, α^+, constant within the range of Reynolds numbers investigated herein is of special significance. Two cases were studied: that of $\alpha^+ = 0.1$ and $\alpha^+ = 0.2$. As can be seen from Table 1, these were obtained by increasing both pitch rate and flow velocity proportionately. Figures 7 and 8 show C_l vs α curves for the respective constant α^+ cases.

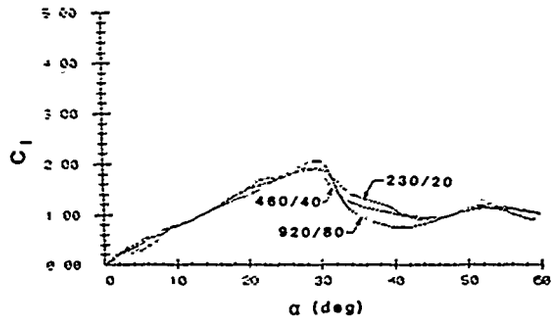

Figure 7. $\alpha^+ = 0.1$, $\dot{\alpha}$ = 230, 460, 920 deg/sec, U_∞ = 20, 40, 80 ft/sec

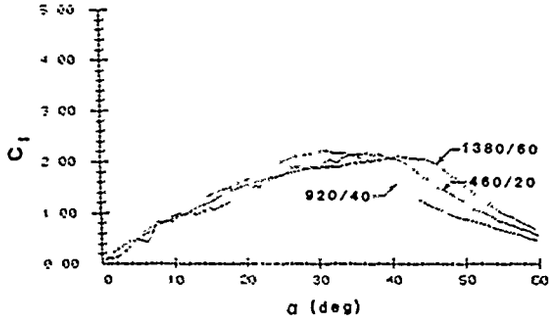

Figure 8. $\alpha^+ = 0.2$, $\dot{\alpha}$ = 460, 920, 1380 deg/sec, U_∞ = 20, 40, 60 ft/sec

As one can readily see, each set of constant α^+ curves are very similar. For $\alpha^+ = 0.1$, each of the three curves start out at a high initial slope for the first two or three degrees, then proceed linearly at a slope of approximately 4.2 until reaching a $C_{l_{max}}$ of about 2.0 at 31 or 32 degrees. The higher pitch rates produce slightly higher $C_{l_{max}}$s at slightly higher angles of attack, but to this point they are virtually the same within the error band of the data. The curves then drop off rapidly - the higher the rotation rate, the sharper the drop with respect to angle of attack - and oscillate about a C_l of 1.2 out to 60 degrees. The three lift curves at $\alpha^+ = 0.2$ do not behave in quite the same manner as those at $\alpha^+ = 0.1$. They start out for the first 20 degrees or so with the same slopes as one another but not, as with the lower value, linear. They then deviate somewhat from one another, peaking out at the same value of $C_{l_{max}}$ of 2.2, but at angles of attack varying from 31 to 41 degrees. There seems to be no specific trend which can be attributed to either rotation rate or flow velocity, since the curve that appears to be in the middle is actually that for the lowest pitch rate. At these high pitch rates this minor anomaly could be attributed to experimental error. The conclusion remains, however, that the non-dimensional pitch rate parameter, α^+ is at this point, the major determining factor for the shape and magnitude of the lift curve. Thus, since curves of constant α^+ are nearly similar, examining the effects of changing α^+ is closely akin to analyzing the effects of changing the pitch rate at constant Reynolds number as in Figure 3. One can see from there and from Figures 7 and 8 that increasing α^+ results in increases in $dC_l/d\alpha$, $C_{l_{max}}$, and α at $C_{l_{max}}$. In addition, lower values of α^+ result in more abrupt decreases in C_l occurring after having reached $C_{l_{max}}$.

Pressure Coefficient vs x/c: The Appendix contains Figures A.1 (a), (b), (c), (d) through A.9 (a), (b), (c), (d). The numbers 1-9 correspond to each of the cases shown in Table 1 starting with U_∞ = 20 ft/sec, $\dot{\alpha}$ = 230 deg/sec, $\alpha^+ = 0.1$, following left to right and ending with U_∞ = 80 ft/sec, $\dot{\alpha}$ = 920 deg/sec, $\alpha^+ = 0.1$. The (a) - (d) discriminants refer to angles of attack of 15°, 30°, 45°, and 60° respectively.

Walker et. al.[14] presented qualitative data using a smoke-wire flow visualization technique and near-surface single element hot-film velocity magnitude measurements for two cases essentially the same as two of the cases examined herein: $\alpha^+ = 0.2$ and 0.6. In these experiments they observed strong vortices forming above the suction surface of the airfoil due to the shear layer interaction between the freestream and the leading edge separation bubble formed as the airfoil pitches up and to the added rotational energy imparted to the flow. They were able to correlate the movements of these vortices with velocity magnitude peaks measured with the hot-film sensors. Figures A.2 and A.4 show the corresponding surface pressure measurement experiments to these two cases; and the upper surface pressure peaks are in good agreement with the spatial positions of the vortices.

Figure A.1 is for the case of the lowest pitch rate examined corresponding to an α^+ of 0.1. Except for the fact that the NACA 0015 airfoil would be stalled at 15 degrees in steady flow, (a) shows a rather ordinary C_p plot for high angles of attack, with the exception of the first 20% of the upper surface. Here one can observe a pressure peak at the 16% chord point indicating the presence of the leading edge vortex. Also, there is no high suction peak very near the leading edge that is present in steady flow. This is true for all of the other cases studied with the exception of the lowest ($\alpha^+ = 0.05$) case. This

is apparently due to the interaction of the leading edge vortex reverse flow in the vicinity of the leading edge and the freestream flow producing locally reduced flow velocities. In (b) we can see that the vortex is still producing a great deal of lift and has traversed to a point slightly aft of mid-chord. In (c) we can now tell that the vortex has separated from the airfoil causing it to stall.

Increasing α^+ to a value of 0.2, Figure A.2 (a) shows characteristics similar to A.1 (a) but higher in value; and then (b) shows a very high pressure peak of almost -6.0 at 24% chord indicating the presence of a stronger vortex than previously observed. By the time the airfoil reaches 45° in (c), the vortex has moved past mid-chord and away from the airfoil, substantially reducing lift. At 60°, the airfoil is completely stalled. Also, an interesting pressure anomaly has entered the picture.

From 8% to 56% chord at an angle of attack of 45°, the lower surface pressure coefficient is slightly greater than one. This could be attributed to experimental error except for two things: Francis, et. al.[11] noticed this sort of phenomenon in their experiments and stated that it should be investigated further; and in the sets of experiments reported herein, this phenomenon is observed to become more pronounced at higher angles of attack and at higher values of α^+. It appears to occur at α^+ levels of 0.2 or greater, where a great deal of rotational energy relative to the freestream is injected into the flow producing large flow curvatures. King[19] has pointed out that a V/r term from Crocco's theorem as presented in Liepmann and Roshko[20] may be the culprit by increasing the local stagnation pressure.

For the case of $\alpha^+ = 0.4$, Figures A.3 (a) indicates a very high value of C_p over the entire airfoil similar in nature for the previous case but greater in magnitude. At an angle of attack of 30°, (b) shows a very large peak in C_p of greater than -9.0 at the 10% chord point. By the time the airfoil has reached an angle of attack of 45° in (c), the vortex has moved downstream to the 34% chord point and away from the airfoil. At 60°, shown in (d), the vortex has moved further downstream but is still exhibiting a great deal of influence on the flowfield around the airfoil.

Figure A.4 depicts pressure coefficients for the last of the four cases at $U_\infty = 20$ ft/sec. This is the case of the highest α^+ examined. At $\alpha^+ = 0.6$ the airfoil is pitching up at a rate of 1380 deg/sec. At 15° in (a), the C_p curve looks about the same as the previous case except a bit higher. In (b), the vortex hasn't really formed yet, but the pressure peak at 6% chord is at -9.8 and the flow is still attached over the entire airfoil. In addition, the maximum lower surface pressure coefficient has reached 1.5. By 45° the vortex has fully formed producing a pressure peak greater than -14.0 at the 14% chord point. These conditions have also resulted in a maximum lower surface C_p of 2.0 at 47% chord. As the airfoil reaches 60° in (d), the vortex has moved to 24% chord. As the airfoil reaches 60° in (d), the vortex has moved to 24% chord and away from the surface resulting in a reduced C_p of -9.0.

Figures A.5 and A.6 show pressure coefficients for two pitch rates at U_∞ = 40 ft/sec corresponding to non-dimensional pitch rates of 0.1 and 0.2 respectively. They are remarkably similar to Figures A.1 and A.2 with only minor differences in peak values and locations.

The only data taken at 60 ft/sec are for $\alpha^+ = 0.2$ with a corresponding pitch rate of 1380 deg/sec shown in Figure A.7. Again, as with Figure A.6, the pressure coefficient data is very similar to that of Figure A.2 - the only exception being that of A.7 (c), where a relatively high peak is seen at 34% chord.

Two final sets of experimental data were taken at $U_\infty = 80$ ft/sec. These are shown in Figures A.8 and A.9 for α^+ values of 0.05 and 0.1 respectively. In A.8 (a) we see C_p curves much like those of unstalled high angles of attack for this airfoil. At 30° it is apparant that the airfoil has stalled completely, indicating that the leading edge vortex has either not formed or does not have the requisite strength to produce the strong reverse flow velocities observed previously.

Figures A.9 (a), (c), and (d) look very much like their same α^+ counterparts in Figures A.2 and A.5. A.9 (b), however, is somewhat differen Whereas the first two cases where $\alpha^+ = 0.1$ at an angle of attack of 30° produced suction surface pressure coefficients of -1.5 to -1.8 near the leading edge, increasing to -3.5 at 47% to 53% chord, and dropping to -0.5 at 85% chord, this one starts at -3.0 near the leading edge, peaks at -4.0 at 34% chord, and falls rapidly to -0.5 at 65% chord. While this will produce almost the same lift coefficients, the indication in this case is that the leading edge vortex develops somewhat more rapidly and is somewhat stronger than in the previous $\alpha^+ = 0.1$ cases. Additionally, a greater portion of the aft section of the airfoil is separated.

Conclusions

The experimental pressure measurements presented herein have shown relationships between the unsteady lifting forces on a pitching airfoil and pitch rate, Reynolds number, and non-dimensional pitch rate, α^+. With regard to lift coefficients it was seen that, for constant Reynolds number (or flow velocity), increasing pitch rate (or non-dimensional pitch rate) increased $C_{l_{max}}$, $dC_l/d\alpha$ up to $C_{l_{max}}$, and, in general, the angle of attack at which $C_{l_{max}}$ occurs. These effects were more dramatic at lower Reynolds numbers. Increasing Reynolds number while holding pitch rate constant had the opposite effect. The effect of holding the non-dimensional pitch rate constant while allowing pitch rate and Reynolds number (flow velocity) to vary is of special interest. For both cases studied, $\alpha^+ = 0.1$ and 0.2, the C_l vs α curves were very similar at constant α^+ - only the angle of attack for $C_{l_{max}}$ showed inconsistencies at the higher value.

Examination of the non-integrated parameters, the pressure coefficients, proved physically enlightening. Not only did the C_p vs x/c curves show the same overall effects as the C_l vs α curves with regard to changes in pitch rate, Reynolds number and non-dimensional pitch rate, but for constant α^+ values the pressure coefficient curves were similar in value over the entire airfoil. In addition, the movement of the "dynamic stall" vortices and their effects on the airfoil under different conditions showed a close and predictable interaction between the major flowfield structure educed and the aerodynamic forces generated. More comprehensive experiments should provide the basis for modeling criteria as well as for technologies leading to successful utilization of the dynamic stall vortices.

References

1. McCroskey, W.J., "Unsteady Airfoils," Annual Review of Fluid Mechanics, pp 285-311, 1982.
2. Herbst, W.B., "Supermaneuverability," Joint Automatic Control Conference, Univ. of VA, 17-19 Jun 1981; see also Workshop on Unsteady Separated Flow, USAF Academy, 10-11 Aug 1983, published by the Univ. of CO Dept of Aero. Engr. Sci.
3. McCroskey, W.J., and Philippe, J.J., "Unsteady Viscous Flow on Oscillating Airfoils," AIAA J., Vol. 13, No. 1, pp 71-79, Jan 1975.
4. McAlister, K.W., and Carr, L.W., "Water Tunnel Visualization of Dynamic Stall," J. Fluids Engr., Vol. 101, pp 376-380, Sep 1978.
5. Martin, J.M, Empey, R.W., McCroskey, W.J., and Caradonna, F.X., "An Experimental Analysis of Dynamic Stall on an Oscillating Airfoil," J. Am. Hel. Soc., Vol. 19, No. 1, pp 26-32, Jan 1973.
6. Robinson, M.C., and Luttges, M.W., "Unsteady Flow Separation and Attachment Induced by Pitching Airfoils," AIAA Paper 83-0131, Jan 1983.
7. Robinson, M.C., and Luttges, M.W., "Unsteady Separated Flow: Forced and Common Vorticity About Oscillating Airfoils," Workshop on Unsteady Separated Flows, pp 117-126, USAF Academy, 10-11 Aug 1983, published by the Univ. of CO Dept. of Aero. Engr. Sci.
8. Carr, L.W., McAlister, K.W., and McCroskey, W.J., "Analysis of the Development of Dynamic Stall Based on Oscillating Airfoil Experiments," NASA TN D-8382, Jan 1977.
9. Harper, P.W., and Flanigan, R.E., "The Effect of Rate Change of Angle of Attack on the Maximum Lift of a Small Model," NACA TN 2061, 1950.
10. Ham, N.D., and Garelick, M.S., "Dynamic Stall Considerations in Helicopter Rotors," J. Am. Hel. Soc., pp 40-50, Apr 1968.
11. Francis, M.S., Keesee, J.E., and Retelle, J.P., "An Investigation of Airfoil Dynamic Stall with Large Amplitude Motion," FJSRL-TR-83-0010, Oct 1983.
12. Deekins, A.C., and Kuebler, W.R., "A Smoke Tunnel Investigation of Dynamic Separating," Aeronautics Digest, USAFA-TR-79-1, pp 2-16. Feb 1979.
13. Daley, D.C., "The Experimental Investigation of Dynamic Stall," Thesis, AFIT/GAE/AA/820-6, Air Force Inst. Of Tech., WPAFB, OH, 1983.
14. Walker, J.M., Helin, H.E., and Strickland, J.H., "An Experimental Investigation of an Airfoil Undergoing Large Amplitude Pitching Motions," AIAA Paper 85-0039, The Aerospace Sciences Conference, Reno, NV, Jan 1985.
15. Helin, H.E., and Walker, J.M., "Interrelated Effects of Pitch Rate and Pivot Point on Airfoil Dynamic Stall," AIAA Paper 85-0130, The Aerospace Sciences Conference, Reno, NM, Jan 1985.
16. Francis, M.S., Keesee, J.E., and Retelle, J.P., "A Two-Degree-of-Freedom Oscillator for Unsteady Aerodynamics Applications," FJSRL-TR-81-0007, Jul 1981.
17. Gormont, R.E., "A Mathematical Model of Unsteady Aerodynamics and Radial Flow for Application to Helicopter Rotors," U.S. Army AMRDL Technical Report 72-67, 1973.
18. Strickland, J.H., and Graham, G.M., "A Dynamic Stall Inception Correlation for Airfoils Undergoing constant Pitch Rate Motions,"

Technical Note submitted to AIAA for publication in AIAA J., Sep 1984.

19. King, P., private conversation, Jan 1985.

20. Liepmann, H.W., and Roshko, A., Elements of Gas Dynamics, Galcit Aeronautical Series, John Wiley and Sons, Inc., New York, 1957.

Appendix

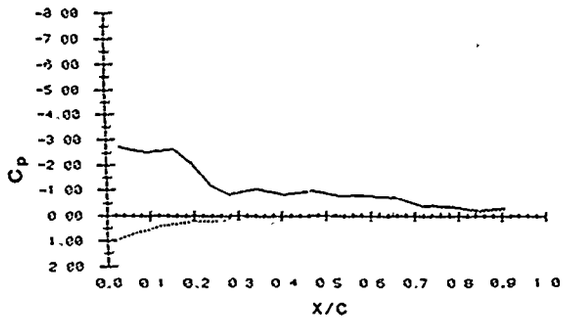

a) 15°

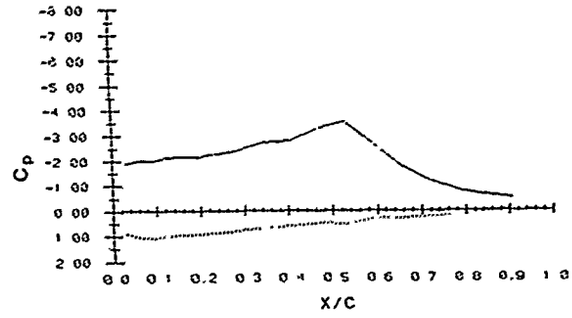

b) 30°

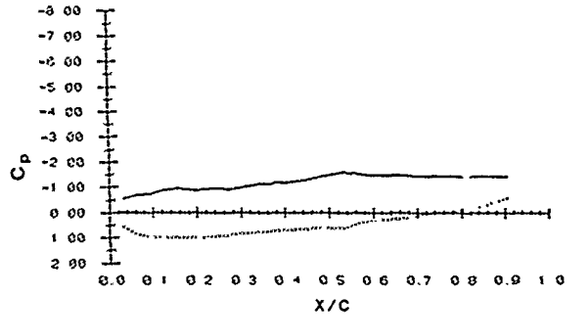

c) 45°

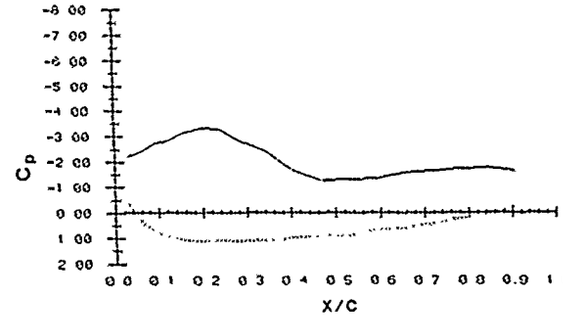

d) 60°

Figure A.1 $\alpha^+ = 0.1$, $\dot{\alpha} = 230^\circ/s$, $U_\infty = 20$ f/s

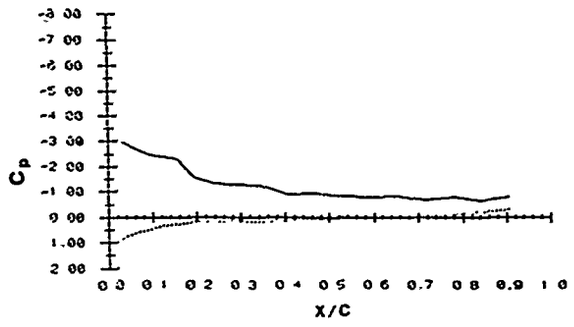

a) 15°

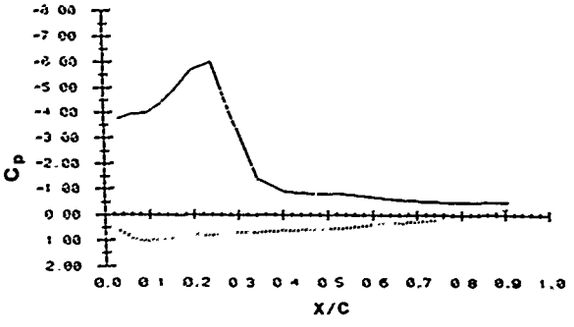

b) 30°

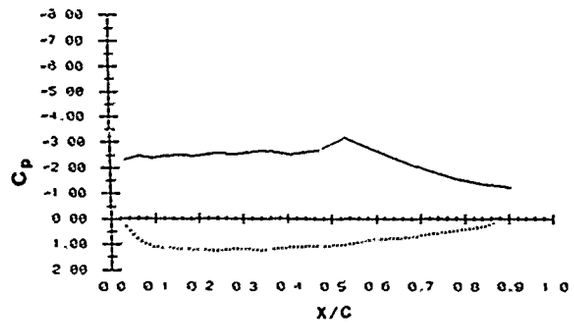

c) 45°

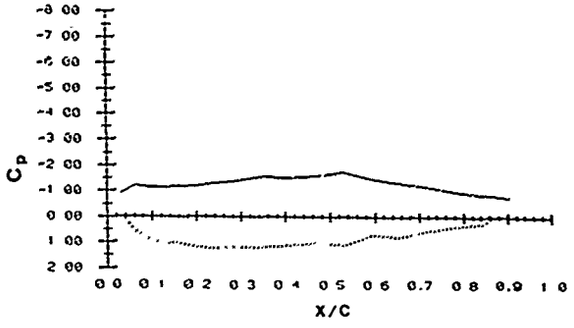

d) 60°

Figure A.2 $\alpha^{+} = 0.2, \dot{\alpha} = 460^{\circ}/s, U_{\infty} = 20$ f/s

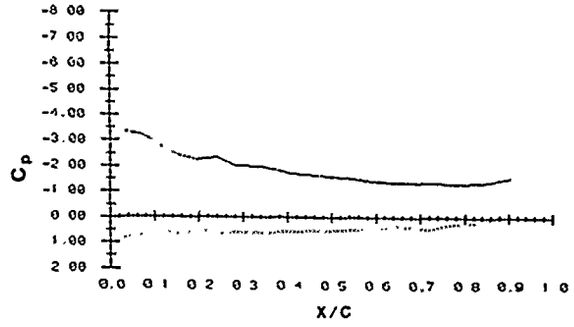

a) 15°

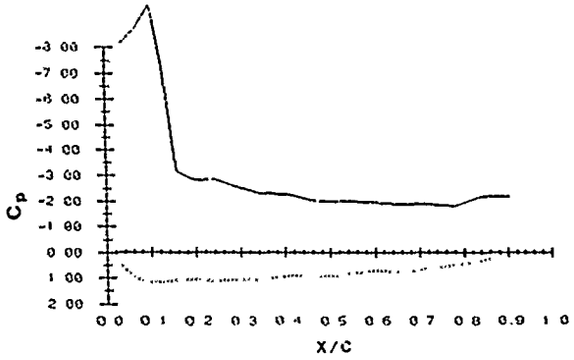

b) 30°

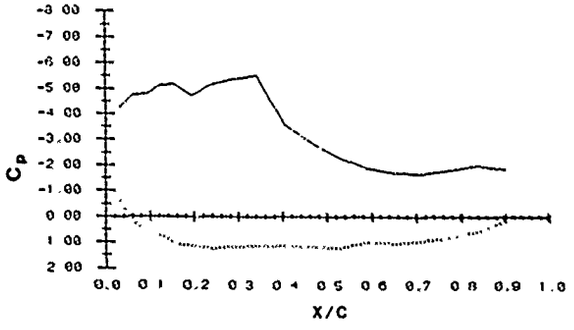

c) 45°

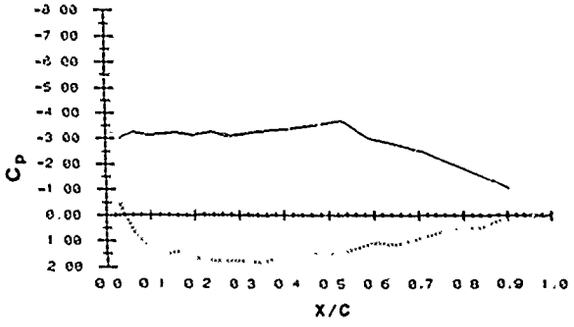

d) 60°

Figure A.3 $\alpha^{+} = 0.4, \dot{\alpha} = 920^{\circ}/s, U_{\infty} = 20$ f/s

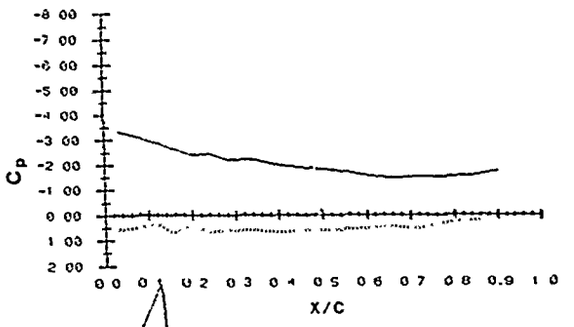

a) 15°

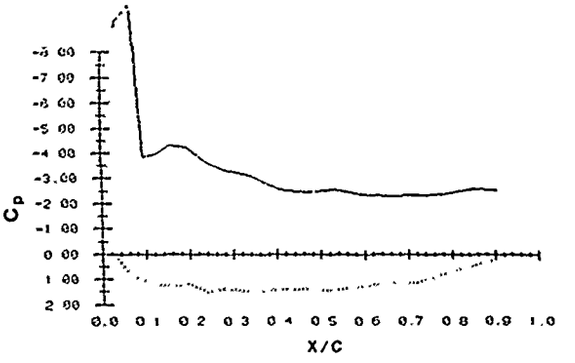

b) 30°

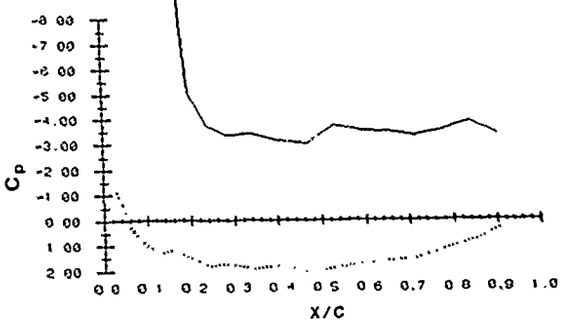

c) 45°

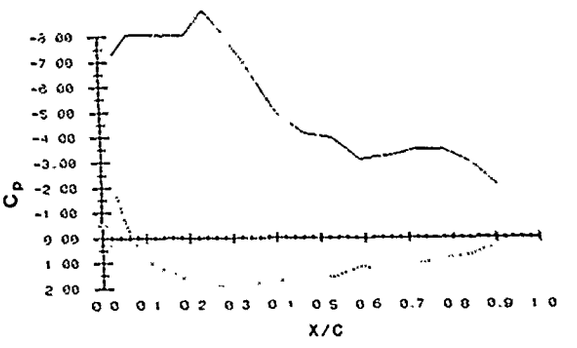

d) 60°

Figure A.4 $\alpha^+ = 0.6$, $\dot{\alpha} = 1380^\circ/s$, $U_\infty = 20$ f/s

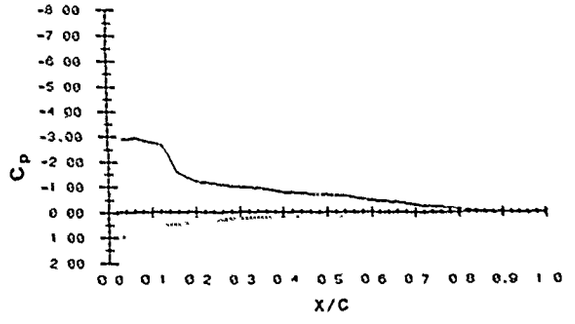

a) 15°

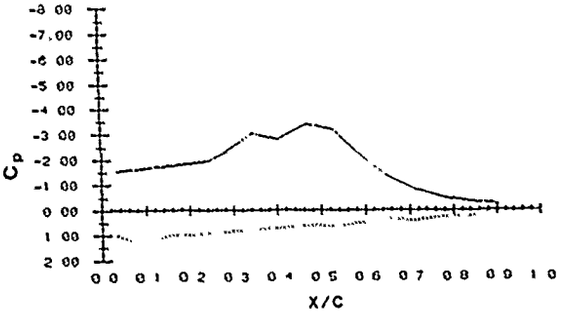

b) 30°

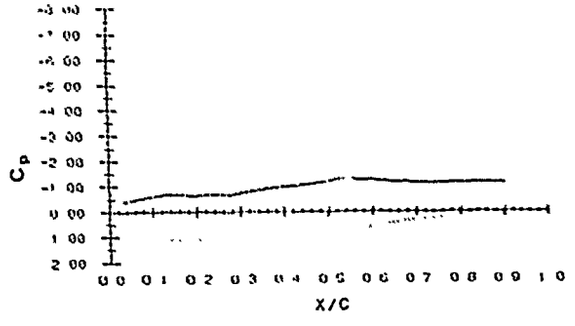

c) 45°

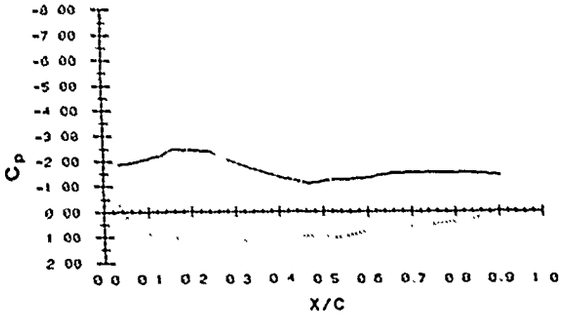

d) 60°

Figure A.5 $\alpha^+ = 0.1$, $\dot{\alpha} = 460^\circ/s$, $U_\infty = 40$ f/s

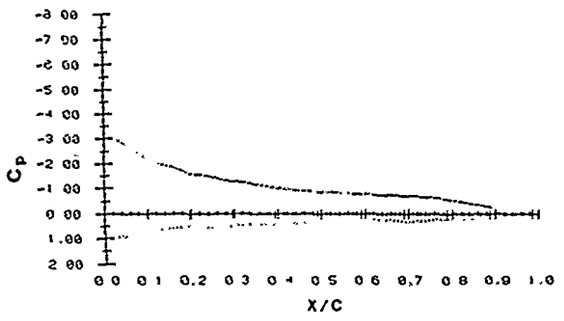

a) 15°

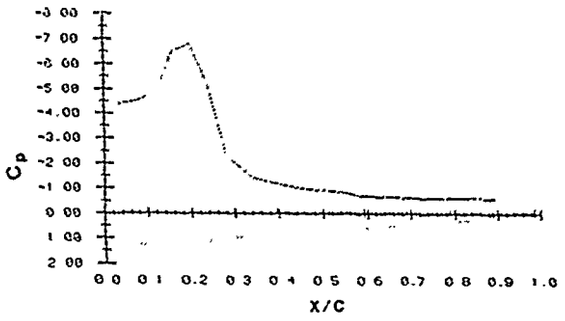

b) 30°

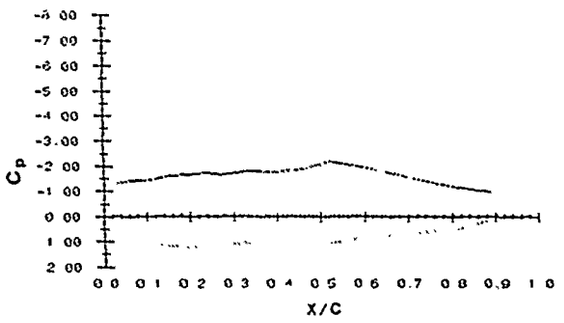

c) 45°

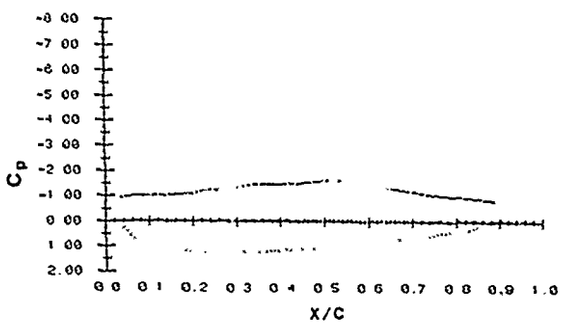

d) 60°

Figure A.6 $\alpha^+ = 0.2$, $\dot{\alpha} = 920^\circ/s$, $U_\infty = 40$ f/s

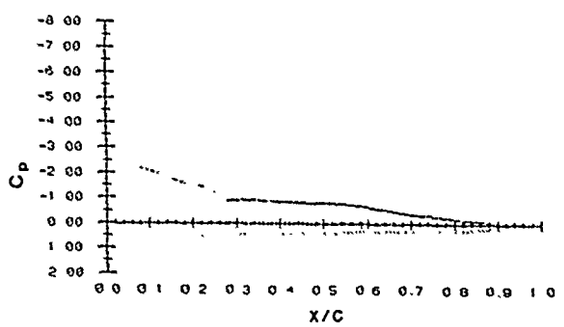

a) 15°

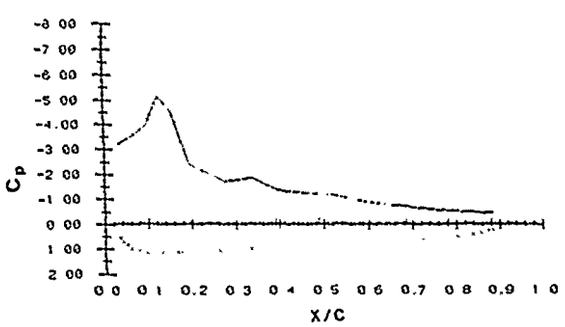

b) 30°

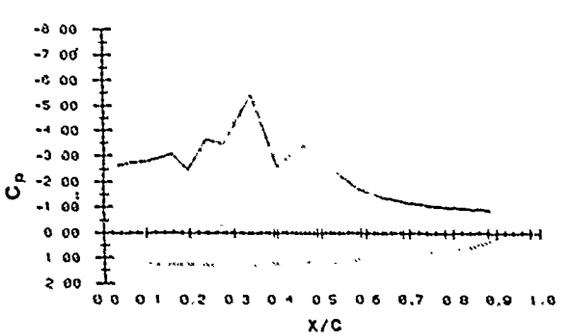

c) 45°

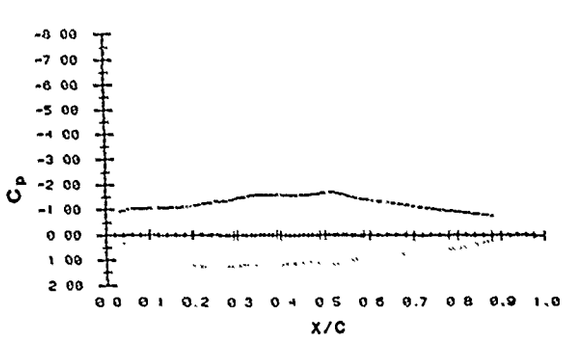

d) 60°

Figure A.7 $\alpha^+ = 0.2$, $\dot{\alpha} = 1380^\circ/s$, $U_\infty = 60$ f/s

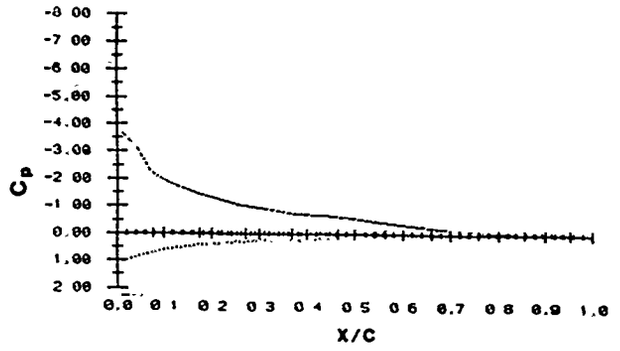

a) 15°

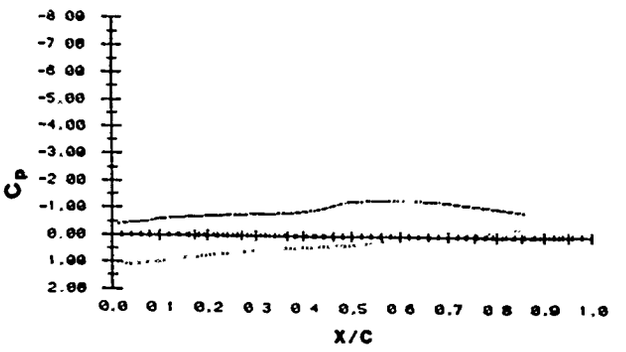

b) 30°

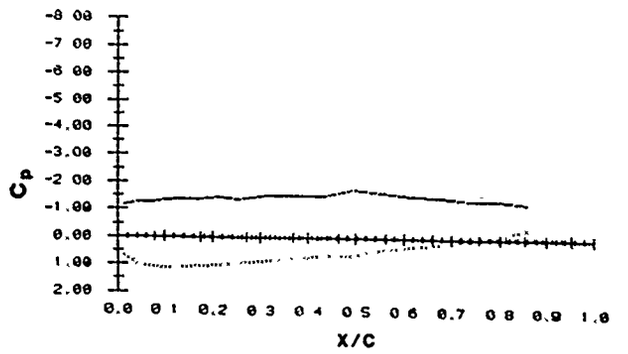

c) 45°

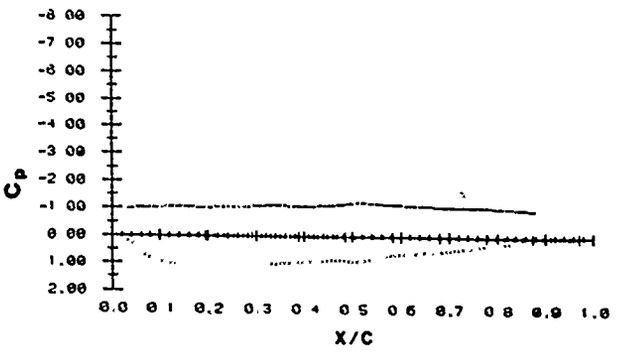

d) 60°

Figure A.8 $\alpha^+ = 0.05$, $\dot{\alpha} = 460^\circ/s$, $U_\infty = 60$ f/s

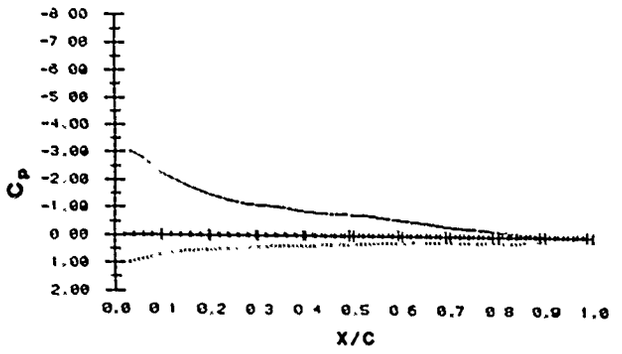

a) 15°

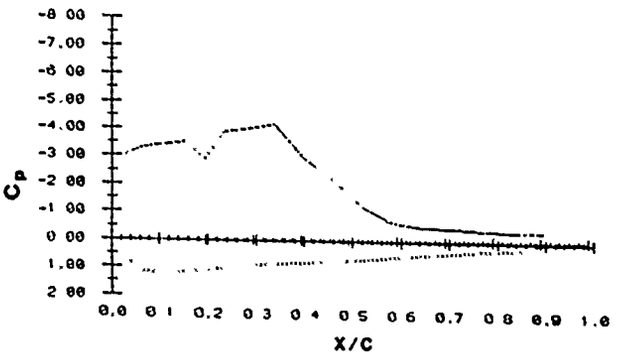

b) 30°

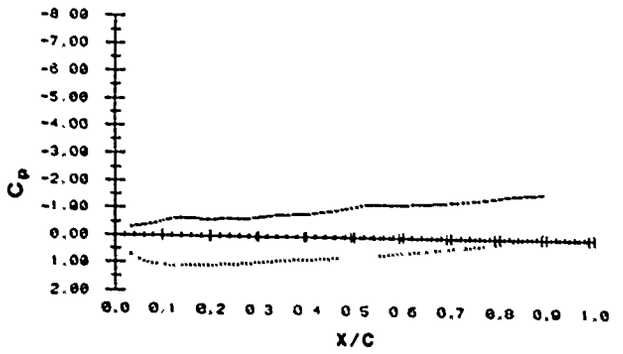

c) 45°

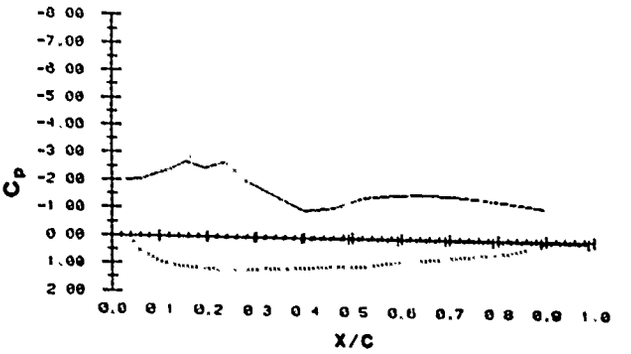

d) 60°

Figure A.9 $\alpha^+ = 0.1$, $\dot{\alpha} = 920^\circ/s$, $U_\infty = 80$ f/s